Journal of Sustainable Metallurgy (2022) 8:613–624
https://doi.org/10.1007/s40831-022-00526-8

REVIEW ARTICLE

Wettable TiB_2 Cathode for Aluminum Electrolysis: A Review

Sai Krishna Padamata[1] · Kamaljeet Singh[1,2] · Geir Martin Haarberg[2] · Gudrun Saevarsdottir[1,2]

Received: 29 December 2021 / Accepted: 30 March 2022 / Published online: 2 May 2022

Abstract

Titanium diboride (TiB_2) is considered a promising material for wettable cathodes in aluminum electrolysis. The demand for wettable cathodes is associated with the development of inert anode technologies to eliminate CO_2 emissions caused by the conventional aluminum reduction process. Titanium diboride has been given special attention due to its superior properties, such as high wettability, good electrical conductivity, wear resistance, and excellent chemical stability. In this paper, we discuss different synthesis techniques used for the preparation of TiB_2 cathode material. The main methods are sintering, electrodeposition, and plasma spraying. Electrodeposition is considered to be the most reliable low-cost method for TiB_2 preparation. The vertical anode–cathode distance can be reduced by introducing wetted TiB_2 cathodes, through which specific energy consumption can be reduced significantly. For a longer lifetime, the TiB_2 cathodes should be resistant to electrolyte penetration. Further research should be conducted to understand the electrochemical behavior of TiB_2 in low-temperature electrolytes.

The contributing editor for this article was Adam Clayton Powell.

✉ Gudrun Saevarsdottir
gudrunsa@ru.is

[1] Department of Engineering, Reykjavik University, 102 Reykjavik, Iceland

[2] Department of Materials Science and Engineering, NTNU, 7491 Trondheim, Norway

Graphical Abstract

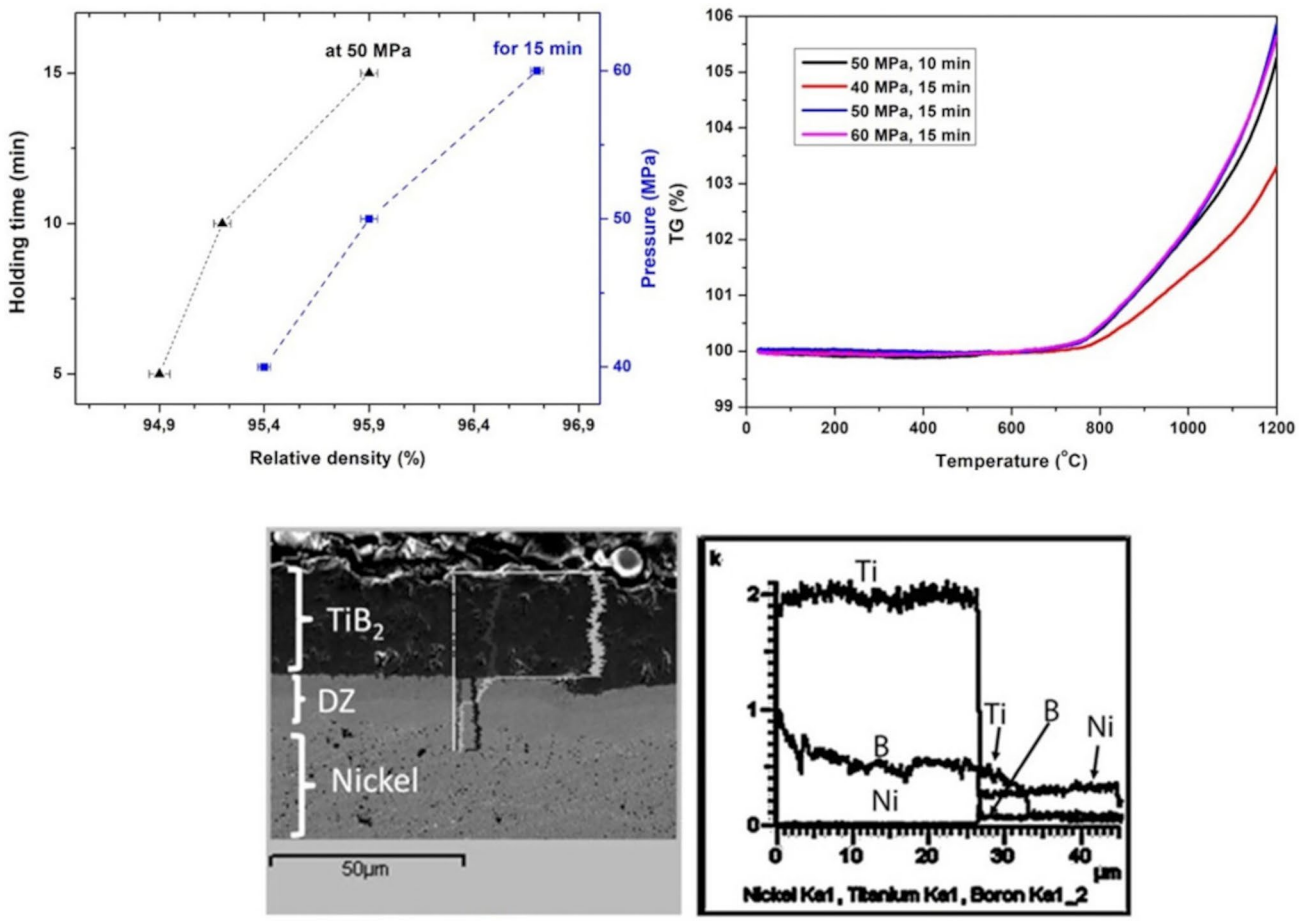

Keywords Titanium diboride · Electrodeposition · Wettability · Aluminum reduction · Wettable cathode · Molten salts

Introduction

The Hall–Heroult process has been the main technology for aluminum production for more than 130 years. In this process, a consumable carbon anode and carbon cathode (covered with liquid aluminum) are used with a cryolite-based electrolyte. The following reaction takes place where the alumina raw material, dissolved in the electrolyte, is reduced to aluminum

$$3C_{(s)} + 2Al_2O_{3(diss)} \rightarrow 4Al_{(l)} + 3CO_{2(g)} \quad (1)$$

The Hall–Heroult process is associated with high energy consumption and high amounts of carbon dioxide and greenhouse gas emissions. About 1.5 t CO_2/t of Al is emitted during the electrowinning of aluminum, of which 0.2 t CO_2/t of Al comes from perfluorocarbon gas emissions [1], arising from the anode effect and consumption of prebaked carbon anode. In addition to 1.5 t CO_2/t, about 0.6 t CO_2/t of Al corresponds to the preparation of prebaked carbon anodes. Specific energy consumption is 12500 – 16,000 kWh/ t of Al for the electrochemical decomposition of alumina compared to the theoretical value of 6330 kWh/ t of Al [2] required to supply the enthalpy for the reaction. The surplus energy is lost in the form of heat.

Replacing consumable carbon anodes with inert anodes can eliminate CO_2 emissions from the electrolysis process. The following reaction takes place by using inert anodes:

$$2Al_2O_{3(diss)} \rightarrow 4Al_{(l)} + 3O_{2(g)} \quad (2)$$

However, the usage of inert anodes for aluminum production requires many changes in cell design and operating conditions. The inert anodes at low temperatures (around 800 °C) would be less prone to corrosion and thermal shocks. As the chemical energy in carbon is absent from the inert anode system, a cell with inert anodes would have a cell voltage of more than 1 V higher than the one with

carbon anodes if no other changes were made to the process design. This would increase the specific energy consumption [3]. Using a vertical electrodes cell (VEC) allows a reduction of the cell voltage by minimizing the anode–cathode distance (ACD) and thus resistive losses. Using VEC with inert anodes can reduce the specific energy consumption by up to 30% [4].

VEC requires a cathode with high wettability towards Al to minimize the ACD to maintain low cell voltage. In the Hall–Heroult process, the cathode is covered with about 20 cm aluminum liquid, which serves as a functional cathode. As the electric current passes through the cell, it interacts with the magnetic field in the potroom, electromagnetic forces lead to the molten aluminum flow and waves in the metal–electrolyte interface, resulting in a risk of short-circuiting between the aluminum and the anode. To avoid short-circulating, a minimum of 4 to 6 cm ACD is maintained in the cell. For efficient cathodic deposition, it is desirable to maintain a molten aluminum cathode in the vertical anode–cathode system, so in the absence of a liquid metal pool, a wettable inert cathode, which is entirely wetted by liquid aluminum, is required. A stable 0.3-cm-thick layer of liquid aluminum on a wettable cathode can keep the cathode inert and protected [5].

Titanium diboride (TiB_2) is considered the most suitable cathode material due to its excellent wettability with molten Al, the low wear rate of 0.25 mm/year in aluminum, resistance towards oxidation at elevated temperatures, high wear resistance and hardness, resistance to corrosion from cryolite melts, and superior electrical conductivity of $9-15\times10^5$ S/cm [6, 7]. A wettable TiB_2 can reduce the ohmic voltage drop, as this cathode material can work at low ACD, eventually decreasing the specific energy consumption [8]. The two main backdrops of using the TiB_2 are the high production cost and the thermal shocks caused due to the strong covalent bonds between the B and B atoms and the ionic bond between the Ti and B atoms [9]. In this review, we discuss the synthesis methods used in the fabrication of TiB_2 cathodes, properties of TiB_2 such as wettability and corrosion behavior, and finally, the environmental and economic impact of using TiB_2 cathodes.

Preparation of TiB_2 Cathodes

TiB_2 Ceramic Materials

TiB_2 has poor sinterability, making it complex to fabricate components with dense and large sizes. One of the contributing factors for the poor sinterability of TiB_2 is the presence of TiO_2 and B_2O_3 oxide layers on the surface, causing difficulties in the densification of TiB_2 samples. TiB_2 can withstand high temperatures as both covalent (B–B) and ionic (Ti–B) bonds exist. The densification of the TiB_2 is limited by its low self-diffusion coefficient. TiB_2 material with a relative density of more than 95% can be fabricated through hot pressing and pressureless sintering or a cold press followed by high-temperature sintering [5].

Kang and Kim [10] were successful in performing pressureless sintering of TiB_2 powder with an average particle size of 0.9 µm at two different temperatures (1800 and 1900 °C) for 2 h to obtain TiB_2. As a sintering aid, 0.5 wt% of Cr and Fe were added to the TiB_2 powder, followed by 30 min of spex-milling. TEM examination showed that the Ti–Cr–Fe phase existed at a triple junction. Additions of Cr and Fe were found to enhance the densification of the samples. The specimen sintered at 1800 °C possessed better mechanical properties compared to the specimen sintered at 1900 °C. The relative densities of sintered TiB_2 at 1800 °C and 1900 °C were 97.6% and 98.8%, respectively. However, the specimen sintered at 1900 °C has a grain size larger than 50 µm, which leads to preferential grain growth on the surface. Similar observations were found by Jensen et al.[11], where TiB_2 sample obtained after hot-pressed at sintering temperature of 1800 °C had signs of preferential grain growth. The anisotropy of TiB_2 leads to preferential grain growth, where the anisotropy is due to the difference in thermal expansion and isothermal compressibility across the a axis and c axis [11]. The preferential grain growth at the TiB_2 surface can be avoided by sintering below 1800 °C.

Heidari et al. [12] used Ti and Fe with a wt ratio of 7:3 additives in a pressureless sintering process to perform the sintering at a temperature lower than 1700 °C. Initially, the material was sintered at 1150 °C, followed by ball milling for 1 h. The TiB_2 (90 wt%) and Ti_7Fe_3 (10 wt%) were ball-milled for 10, 30, 60, 120, and 240 min to find the effect of milling on the properties of TiB_2 composite. The milled mixture was sintered under Ar-5%H_2 atmosphere at 1650 °C for 1 h. The specimen made from the 10 min milling had unevenly distributed additives with irregular shapes visible on its surface. The specimen made from the samples milled for 30 min had a uniform microstructure with fine particle size. The relative density of the specimen was 91%. The specimen showed superior electrical conductivity, better wettability by molten Al, and was crack-free. With 24-h exposure to Al, Al penetrated the TiB_2, but the specimen's geometry remained stable. Although the metallic additives reduce the sintering temperatures significantly and eliminate the preferential grain growth, the additives react with the molten aluminum and dissolve, which leads to secondary phase formation at TiB_2 grain boundaries [13, 14]. This could lead to crack formation and uneven thermal expansion. The hot press process is expensive, while the cold press requires high energy consumption, making these processes unfavorable to produce TiB_2 specimens.

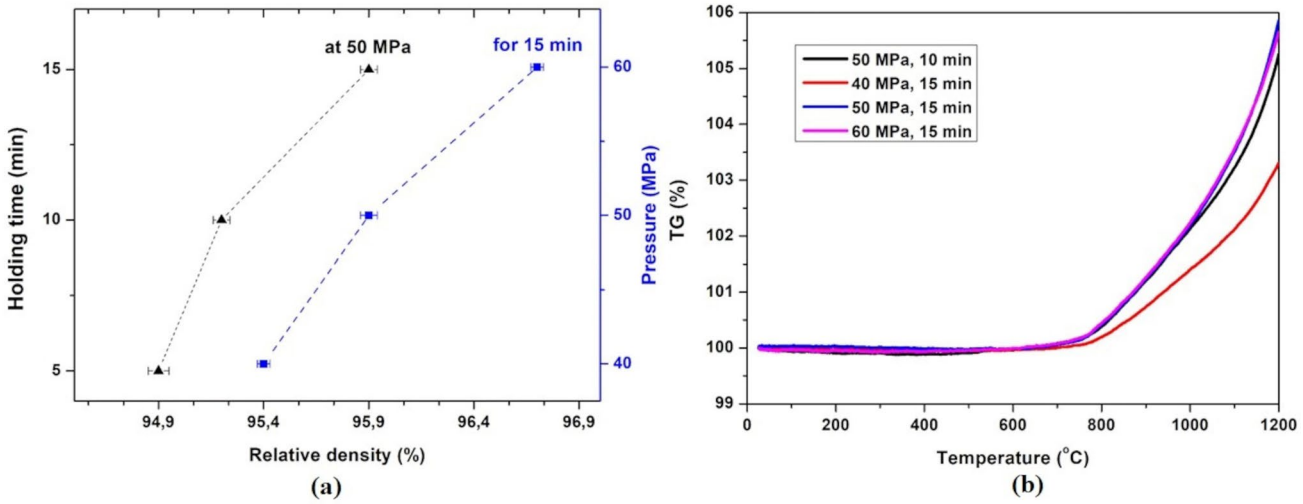

Fig. 1 **a** Relative densities of the TiB_2 samples prepared using SPS at different pressures and holding duration with $T_{max} = 1500$ °C, **b** TG analyses of the samples prepared by SPS, which are heated till 1200 °C under O_2 atmosphere. Reproduced with permission [15]. Copyright 2018, Elsevier

Balci et al. [15] consolidated TiB_2 powder (particle size 0.536 µm, purity ≥ 98.4%) using field-assisted sintering technology/spark plasma sintering (FAST-SPS) process at reduced temperatures around 1500 °C. The TiB_2 used in this process was synthesized from a self-propagating high-temperature synthesis process using a TiO_2–B_2O_3–Mg mixture. Figure 1a shows that the relative density of the TiB_2 prepared from FAST-SPS is influenced by the holding time and pressure applied during sintering. A maximum relative density of 96.7% was obtained when the applied pressure was 60 MPa with a holding time of 15 min. No preferential grain growth was observed on the samples, while the TiB_2 grain size ranged between 2.2 and 6 µm. From Fig. 1b, the TG analysis reveals that the oxidation layer on TiB_2 starts forming after 800 °C.

TiB_2 Coatings

TiB_2 coatings are commonly applied on substrates such as graphite, molybdenum, steel, and nickel. Although graphite is preferred as a suitable substrate due to its thermal expansion coefficient (3.8×10^{-6} K^{-1}) has proximity to TiB_2 expansion value (6×10^{-6} K^{-1}). Zou et al. [16] suggested the TiB_2–SiC coating (via supersonic atmospheric plasma spraying) on a graphite substrate, as the thermal expansion coefficient of the composite layer is much closer to that of graphite, which can minimize the thermal mismatch and reduce the possibility of micro-crack propagation. The adhesiveness between the coating and the substrate is essential for the performance of the coated cathodes. The TiB_2 coating can be achieved mainly using electrodeposition, chemical vapor deposition, and plasma spray technique.

Electrodeposition is considered a cost-efficient and simple method that can be performed at low temperatures around 700 and 1000 °C in molten salts. The electrochemically active precursors dissolved in the molten salts are cathodically deposited on a suitable substrate by applying appropriate potentials or current densities. In TiB_2 electrodeposition, precursors such as KBF_4 (source for B) and K_2TiF_6 (source for Ti) are dissolved in fluoride or chloride melts and reduced on a substrate.

Wendt et al. [17] describe the cathodic deposition of TiB_2 on carbon electrode in FLiNaK melts (eutectic mixture of LiF, KF, and NaF) containing KBF_4 (2 to 10 mol.%) and K_2TiF_6 (2 to 4 mol.%) at 700 °C. The concentration ratio C(B)/C(Ti) ranged between 2 and 3. It was noted that the TiB_2 coating was smooth for layers of thickness of less than 0.05 cm, while the coatings became rougher as the thickness exceeded 0.05 cm. A pure TIB_2 layer can be obtained when the electroreduction is performed at low current densities (around 0.1 A/cm^2). The current efficiency of the process was temperature-dependent and decreased with an increase in the working temperature. Regardless of different thermal expansion coefficients of carbon and TiB_2, an adhesive and strong coating was formed, unlike in the case of a copper substrate where the TiB_2 coating cracked upon cooling. According to the electroreduction mechanism, B is reduced initially on the substrate, followed by the deposition of Ti, leading to the intermetallic bond between the B and Ti [18]. FLiNaK containing KBF_4 and K_2TiF_6 solutes is considered an effective electrolyte due to its good electrochemical window that allows working with active Ti and B ions. It was found that high-purity TiB_2 coatings can be deposited using FLiNaK when the cathode current density is kept under 0.25

A/cm^2. However, one of the biggest advantages of this electrolyte is being highly corrosive [19].

Similarly, Li and Li [20] used FLiNaK melt containing KBF_4 and K_2TiF_6 solutes for cathodic deposition of TiB_2 on molybdenum substrate using continuous current plating (CCP) and periodically interrupted current (PIC) techniques. In the case of CCP, the deposition was performed between current densities of 0.1 and 1 A/cm^2 at 700 °C. Below 0.3 A/cm^2, no TiB_2 was deposited on the substrate, meaning that the overpotential is not high enough for the reduction of Ti and B ions. At current densities between 0.4 and 1.0 A/cm^2, metallic bright deposits were formed, and the surface morphology of coatings was similar. TiB_2 grain size decreased and the coating thickness increased with an increase in cathodic current density. At 0.5 A/cm^2, the TiB_2 was adhesive towards the substrate but the TiB_2 layer was not so compact due to the presence of cracks and pores. Meanwhile, TiB_2 layers deposited at 0.5 A/cm^2 using the PIC technique (frequency = 100 Hz, the current time on/time off = 4/1) contained fine grains and the coating was uniform and compact. Moreover, TiB_2 layers deposited using PIC have lower number of pores with lower diameter. Thus, TiB_2 coating deposited using PIC has superior morphology compared to the one deposited by CCP.

In Makyta et al. [21], it was found that TiB_2 electrodeposition in cryolite-based melts containing KBF_4 and K_2TiF_6 components or the one containing B_2O_3 and TiO_2 was not successful or coherent. The failure corresponds to the thermal deposition of the electrolytes at high temperatures. Meanwhile, a TiB_2 coating with good coherence and adhesion to the substrate was electrodeposited in KF–KCl–KBF_4–K_2TiF_6 melts at 800 °C. The electrodeposition was performed on molybdenum and graphite substrates. The TiB_2 layer formed on the graphite was a perpendicularly growing crystalline structure on the substrate. The thickness of the TiB_2 layer increased with an increase in the cathode current density. However, at high current densities, highly porous and irregularly shaped layers are formed. The governing reaction in the formation of the TiB_2 layer is as follows:

$$2BF_4^- + TiF_6^{3-} + 9e^- \rightarrow TiB_2 + 14F^-. \quad (3)$$

Electrochemical deposition of TiB_2 on graphite in FLiNaK melt was performed at 600 °C using a periodically interrupted current technique by Yvenou et al. [22]. The electrodeposition was conducted at two different current densities, − 0.12 and − 0.50 A/cm^2, for various deposition times (10 to 75 min). As shown in Fig. 2, the coating thickness increases linearly (deposition rate 0.68 µm/min) with time and coincides with the theoretical thickness at $j = -0.12$ A/cm^2. In contrast, the thickness of the layer at j = − 0.50 A/cm^2 grows rapidly (deposition rate 5.8 µm/min)

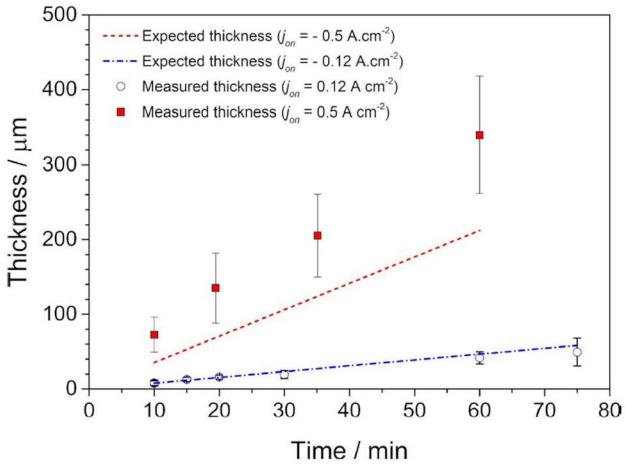

Fig. 2 Representation of the experimentally measured and theoretical thickness of titanium diboride deposits vs. the deposition time. Reproduced with permission [22]. Copyright 2021, John Wiley & Sons

with time. A TiB_2 coating with a denser and preferential crystallographic structure was obtained at $j = -0.12$ A/cm^2. At $j = -0.50$ A/cm^2, a porous layer with numerous microcracks between the coating–substrate interface was observed. It was suggested that a denser and abrasive layer could be obtained at low applied current densities transversal microcracks were obtained, which results in the penetration of molten Al into the coating and culmination of Al.

Ozkalafat et al.[23] electrochemically deposited TiB_2 on nickel substrate in an oxide-type electrolyte containing Ti and B ions. The electrolyte comprises $Na_2B_4O_7$ (94 wt%) and $Na_{16}Ti_{10}O_{28}$ (6 wt%), the source for B and Ti, respectively. The electrodeposition was performed at varying parameters such as current density (0.05–0.150 A/cm^2), temperature (800 − 1000 °C), and deposition time (30 − 360 min) to determine the optimal conditions. XRD methods confirmed the stoichiometry of the TiB_2 layer. The most uniform and thick coating were obtained at a current density of 0.07 A/cm^2. Figure 3a, b shows the consistent distribution of Ti and B across the layer with a composition of 33 at.% Ti and 67 at.% B. The DZ in Fig. 3a represents the diffusion zone where Ti is dissolved in Ni and the formation of nickel boride. The TiB_2 layer thickness increases with time from 3 to 41 µm between 30 and 240 min, as shown in Fig. 3c. At temperatures above 950 °C, nickel diffusion into the TiB_2 coating was observed. Electrodeposition at 850 °C is recommended because at temperatures below, irregular and thin layers are formed with varying Ti:B ratios.

A novel method was proposed by Huang et al. [24] for the synthesis of TiB_2 cathodes. TiB_2–TiB/Ti wettable cathode was prepared by boronizing the Ti substrate in $Na_2B_4O_7$ (75 wt%)–K_2CO_3 (20 wt%)–B_4C (5 wt%) electrolyte. The thickness of the TiB_2 was 10 µm after 3 h of boriding treatment

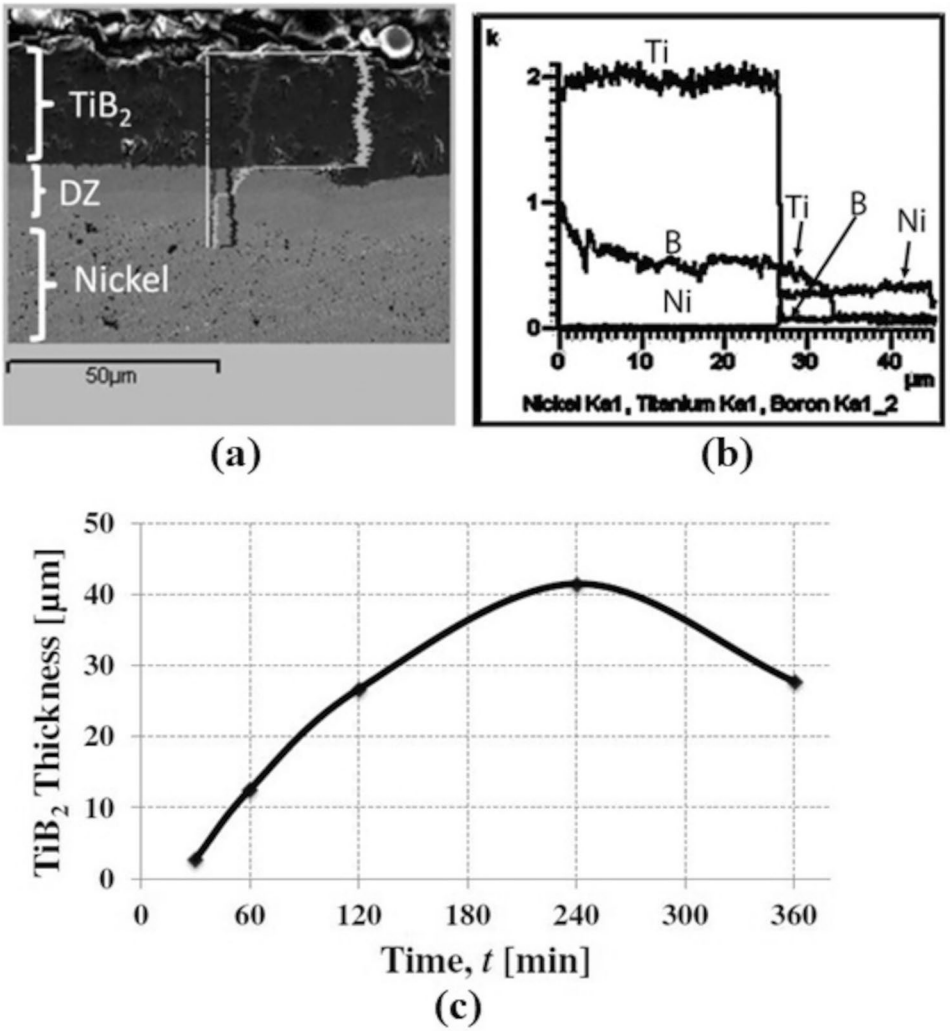

Fig. 3 **a** SEM image, **b** elemental distribution of Ti, B, and Ni, **c** average thickness of TiB_2 coating on Ni substrate at 0.07 A/cm^2 and 850 °C. Reproduced with permission [23]. Copyright 2016, Elsevier

with an applied current density of 0.2 A/cm^2 at 950 °C. The TiB interlayer between the TiB_2 and Ti acts as a binder. The TiB_2 was adhesive to the substrate. The main advantage of using this technique is that the thermal expansions of Ti, TiB, and TiB_2 are similar, resulting in superior binding force at elevated temperatures.

Kartal and Timur [25] synthesized TiB_2 by boriding the titanium using the "Cathodic Reduction and Thermal Diffusion based boriding (CRTD-Bor)" technique. In the CRTD-Bor method, two main steps are involved in the boriding of titanium substrate. Initially, the atomic borons are electrochemically reduced on the surface of the substrate (cathode). This is followed by the adsorption and diffusion of atomic boron on the surface of titanium, resulting in the formation of intermetallics such as TiB and TiB_2. The boriding process was performed in an electrolyte with a composition of 90 wt% borax and 10 wt% sodium carbonate. The process was carried out at varying temperatures (900 °C to 1100 °C) and boriding time (15 min to 120 min) with a constant cathodic current density of 0.2 A/cm^2. Findings suggest that even at low boriding durations (15 min and 30 min), homogeneous thick boride layers containing TiB and TiB_2 phases were formed. SEM cross-sectional micrograph of borided titanium reveals that the top layer was a TiB_2 phase while the intermediate layer between TiB_2 and the titanium substrate was TiB whiskers. The thickness of the TiB_2 layer and the width of TiB whiskers increased with an increase in process temperature. Irrespective of process duration and temperature, the outer TiB_2 layer and TiB whiskers were tightly bonded. The main advantages of this method are the formation of dense and adhesive coating within a short time and being environmentally friendly.

Plasma spray is a well-known technique with a high deposition rate that can be used for TiB_2 coating on different types of substrates [26]. For instance, a fine-lamellar structured TiB_2 with a thickness of 800 µm was deposited on a carbon substrate using the atmosphere plasma spray technique (APS) [27]. However, partial oxidation on the surface of TiB_2 was observed. The coating was made of a matrix combined with fully molten particles and agglomerated

semi-molten TiB_2. The coating by APS is resistant to aluminum carbide formation and sodium penetration [27]. Ananthapadmanabhan et al. [28] conducted oxygen analysis and electrical conductivity measurement on TiB_2 layer on alumina substrates using H_2 plasma. The results show that the TiO_2 and B_2O_3 are formed on the surface, where the oxides are further converted to H_3BO_3. The electrical conductivity was 100 times lower compared to TiB_2 produced from the sintering process. The coating's oxidation behavior and electrical conductive were improved when the plasma spray was performed using Ar-H_2 plasma, which means that the environment of plasma spray influences the behavior of the TiB_2 layers.

Yvenou et al. [29] were the first to deposit micrometric TiB_2 particles on graphite substrate using the suspension plasma spray (SPS) technique. The SPS was performed under the Ar atmosphere to minimize the oxidation of the TiB_2 coating during the process. The results suggest that the use of Ar minimized the TiO_2 and B_2O_3 formation on the layer. The presence of any oxides can enhance the penetration of molten Al into the coating. The SPS TiB_2 coating was cohesive with the graphite substrate. However, it was found that the TiB_2 was porous, and the TiB_2 particles were loosely bonded. The high porosity level is attributed to the TiB_2 particle's low transit time spent in the plasma, resulting in low and uneven melting. It was also found that the Al completely penetrates the coating and reacts with the graphite substrate, thus resulting in weak coherence between the TiB_2 layer and the substrate. A thick TiB_2 coating on a cemented carbide substrate (with 6 wt% Co) was fabricated using direct current magnetron sputtering (DC-MS) by Berger [30]. The deposition was carried out at 6 kW magnetron power, + 50 V substrate bias, and an argon pressure of 3×10^{-3} mbar. The deposition rate of TiB_2 coating was 0.4 µm/min, with a total thickness of 60 µm for 150 min. Scratch test revealed that the TiB_2 coatings showed excellent cohesion to the substrate.

Chemical vapor deposition (CVD) is one of the most common coating techniques where the reactant gases chemically react in an activated (plasma, heating, laser) environment, which results in the formation of stable compounds on the substrates [31]. TiB_2 coatings can be readily deposited on substrates by CVD using different reagents. One of the most common sets of reagents is $TiCl_4$, BCl_3, and H_2. Moers [32] was the first to utilize these reagents for TiB_2 coating, and the following reaction (4) takes place, where the reaction can be efficiently performed at a more comprehensive temperature range of 700 – 1400 °C.

$$TiCl_{4(g)} + 2\,BCl_{3(g)} + 5H_{2(g)} \rightarrow TiB_{2(s)} + 10HCl_{(g)} \quad (4)$$

The orientation of the substrate and the processing conditions influence the crystallographic structure of the TiB_2 layer [33, 34]. Beckloff and Lackey coated TiB_2 layer by CVD technique on graphite substrate using $TiCl_4$, BCl_3, and H_2 reagents [35]. The studies suggest that the TiB_2 grain size increased from 0.5 µm to 3 µm with an increase in deposition temperature from 900 °C to 1100 °C. With decreased BCl_3:$TiCl_4$ ratio and increased deposition temperatures, the grains were oriented parallel to the substrate. Becht et al. [36] observed that the TiB_2 layer depletion occurs when the deposition is performed at a BCl_3:$TiCl_4$ ratio of 8. Pierson and andich suggested that the metallic substrates are not suitable for TiB_2 deposit using CVD, as the metallic substrates can form metallic chlorides, which is undesirable [37].

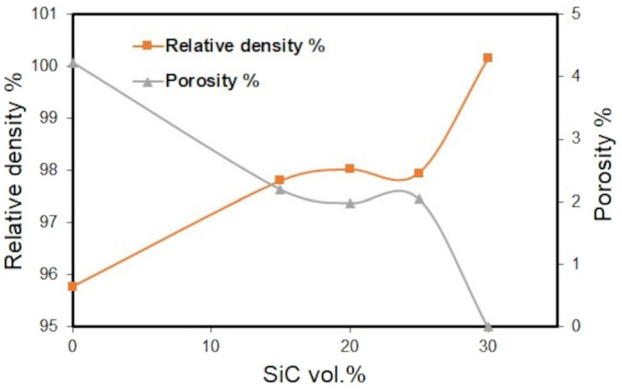

Fig. 4 Represents the influence of SiC on the relative density and porosity of TiB_2 (based on [38])

TiB_2 Composite Cathodes

Composite TiB_2 ceramic materials are of great interest as the pure TiB_2 materials are brittle and are difficult to machine due to their mechanical instability. The addition of other ceramic materials such as TiC, AlN, ZrB_2, and ZrC to TiB_2 can enhance its mechanical properties. Namini et al. [38] studied the influence of SiC addition (15, 20, 25, 30 vol.%) on the mechanical properties of TiB_2 fabricated using vacuum hot pressing technique at 1850 °C for 2 h by applying 20 MPa. Figure 4 shows the influence of SiC vol.% in TiB_2 ceramic composite on relative density and porosity. The studies reveal that composite TiB_2 (70 vol.%) – SiC (30 vol.%) was dense with no porosity. Zhao et al. [39] reported that adding Ni up to 5 wt% could enhance the fracture toughness and hardness of the TiB_2–SiC composite. Moreover, the Ni prevents the anisotropic growth of TiB_2 when prepared by reactive hot pressing.

Wang et al. [40] compared the creep behavior of graphite and TiB_2-graphite (30 wt% TiB_2, 50 wt% C, and 20 wt% binding agents) composite cathodes after specimens were subjected to the electrolysis process in Na_3AlF_6 – KF (5 wt%) – LiF (5 wt%) – Al_2O_3 (8 wt%) at 960 °C with cathode current density 0.5 A/cm^2. It was observed that the TiB_2–C composite had a lower creep strain (0.2%) and

fewer microcracks compared to graphite. The composite was denser, less porous, and was entirely wetted by Al, which would prevent the electrolyte penetration. Fei et al. [41] also observed the superior relative density and flexural strength in TiB_2/C composite compared to pure graphite. An increase of TiB_2 content up to 70 wt% can further improve the wettability of the material and prevent the penetration of Na and bath. However, when the TiB_2 content exceeds 70 wt%, TiO_2 oxide layer forms on the surface of the composite [42]. The electrical resistance of the TiB_2/C composite decreases from 31.2 μΩ to 23.8 μΩ when the TiB_2 concentration increases from 30 to 60 wt% [43]. The electrical resistance decreases with a decrease in the TiB_2 particle size, which could be due to the material's low porosity.

Wettability, Interaction, and Corrosion Behavior of TiB_2

The wettability of TiB_2 by molten Al is dependent on the purity and relative density of the TiB_2 ceramic and temperature during the interaction. The most common method used to study wettability is the sessile drop technique. While looking for a cathode material for a VEC for aluminum electrolysis, the wettability of TiB_2 is excellent (having a sessile drop contact angle ≈ 0°). The dihedral angle equilibrium (5) governs the liquid-phase morphology in the grain boundaries of the solid-phase interface

$$\gamma_B = 2\gamma_{SL}\cos\left(\frac{\theta}{2}\right), \tag{5}$$

where γ_B is the surface energy of the grain boundaries, γ_{SL} is the surface energy of the solid–liquid interphase, and γ_{SL} is the contact angle between the liquid phase and the grain boundary. Figure 5 shows surface forces acting at a point where the liquid phase meets the grain boundary of the solid phase. When γ_{SL} is greater than $0.5\gamma_B$, then the equilibrium will establish a θ greater than zero. When $\theta = 120°$, γ_B is equal to γ_{SL}. However, when γ_{SL} is less than $0.5\gamma_B$, there is no value for θ that goes with Eq. (5), thus no equilibrium is established and liquid will penetrate along with the grain boundaries of solid [44].

Heidari et al. [45] studied the wettability and interaction behavior of porous TiB_2 ceramic (prepared from pressureless sintering [12]) with liquid Al. During the wettability test, for the first 9 min, no visible wetting of Al on TiB_2 was observed at 870 °C. With an increase in temperature to 940 °C (after 22 min), there was a visible wetting with a contact angle of 85°. After 50 min of contact, the contact angle of 6° was measured. The molten Al penetrated the pores of TiB_2, and the additives started dissolving in the Al (see Fig. 6a). Three zones were observed at the Al penetration area (Fig. 6b). The first zone contains Al, the second

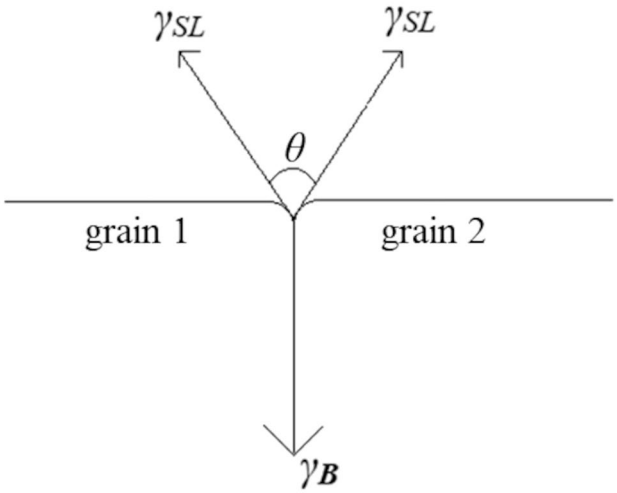

Fig. 5 Equilibrium between a grain boundary in a solid at a solid/liquid interface and the solid/liquid interfacial energies

has $TiAl_3$ phase, and the third zone has $TiAl_3$ and Fe_4Al_{13} phases, while the fourth zone is free of Al (see Fig. 6c). Despite the Al penetration, no significant cracks or change in the geometry of TiB_2 was observed.

Xi et al. [14] studied the wetting and interaction between dense TiB_2 ceramic (relative density of 98.7%) with molten Al between 700 and 1400 °C. Molten Al thoroughly wetted the TiB_2 at temperatures above 1000 °C. Al penetrated TiB_2 up to 250 μm at 1400 °C, Al_xT, Al_4C_3, and Al_2O_3 particles were found between the Al–TiB_2 interface, despite that TiB_2 grains remain attached. Raj and Skyllas-Kazacos examined the wettability of sintered TiB_2 cathodes through the electrolysis process in sodium cryolite melts (Al_2O_3 unsaturated and saturated). TiB_2 cathode showed an excellent wetting property in the unsaturated melt [46]. However, TiB_2 was poorly wetted in the saturated melt due to the TiO_2 and B_2O_3 formation and accumulation on the surface, interfering with Al deposition. Moreover, electrolyte penetration in TiB_2 cathode results in uneven wetting in saturated melts. TiO_2 and B_2O_3 are readily soluble in the unsaturated melt; this could be why the oxide phases were not detected on TiB_2 cathodes tested in unsaturated melts. The wettability of the TiB_2/C composite for the aluminum is time-dependent, as it requires time to remove impurities from the surface of the composite. The contact angle from the molten aluminum on TiB_2/C composite reaches 0° after 90 min at 1000 °C [47].

The molten Al penetrates readily into porous TiB_2, having a relative density of 90%, while the penetration by Al was ten times slower than the TiB_2 with a relative density of 96% [48]. Weirauch et al. [49] studied the wettability of TiB_2 (on different substrates) with molten Al at a constant temperature of 1025 °C. TiB_2 with 99.7% relative density and more than 99.8% purity has an initial contact angle of

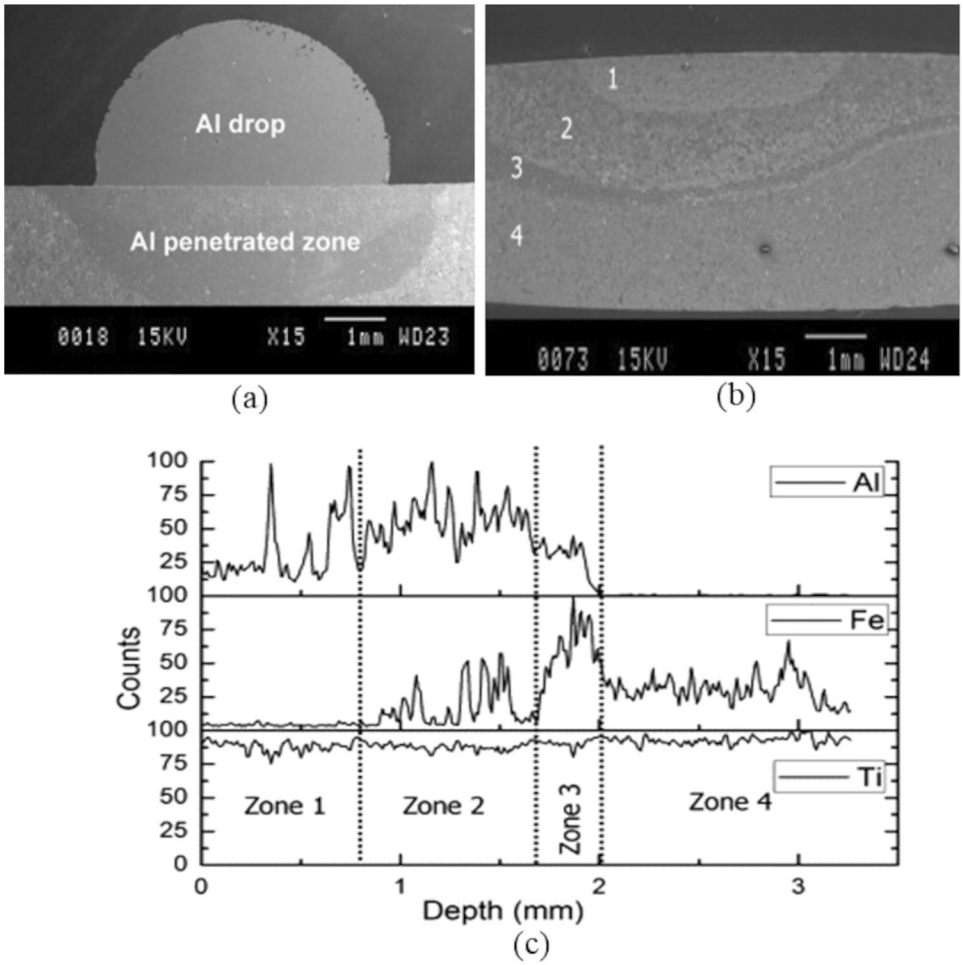

Fig. 6 **a** Back-scattered electron (BSE) micrograph from the cross-sectioning of TiB_2-based specimen with partial penetration of Al, **b** SEM imaging of TiB_2-based specimen after sessile drop test showing different zones, **c** elemental line scans related to the SEM micrograph shown in **b**. Reproduced with permission [45]. Copyright 2012, Elsevier

140° with molten Al, dropped to 0° after 17 h of interaction. Penetration of liquid Al in TiB_2 reduces the flexural strength, hardness, and Young's modulus, resulting in the change of fracture mode from transgranular to intergranular [50]. The surface roughness (0.155 µm − 0.455 µm) of TiB_2 does not influence the wettability of aluminum [51].

Devyatkin and Kaptay investigated the wettability of TiB_2 coating electrodeposited on nickel and carbon substrates from $Na_3AlF_6-Al_4B_2O_9-CaTiO_3$ melt [52]. The thickness of the TiB_2 layer was 20 µm with a deposition rate of 50 µm/h, irrespective of the substrate material. At 1000 °C, after a 4-min contact, the Al and TiB_2 coating (carbon substrate) contact angle was 30°, and the aluminum started penetrating the layer. In the case of TiB_2 coating on nickel substrate, the molten Al had a 0° contact angel, meaning the TiB_2 coating was thoroughly wetted. The solubility of TiB_2 in molten aluminum was estimated to be 6×10^{-3} wt% after 10 h of exposure.

Kontrik et al. [53] investigated the corrosion behavior of TiB_2 (purity ≥ 98%, contains Ni as a sintering aid) in KF-AlF_3–Al_2O_3 melt with cryolite ratio 1.3 and Al_2O_3 3.1 wt% for 50, 100, and 200 h at 680 °C. Pitting corrosion was observed on the TiB_2 material irrespective of its holding time in the melt. After the tests, TiB_2 samples had a small weight gain due to the infiltration of corroded particles into the pores. The Ni-containing grain boundary phase is dissolved gradually, leading to detaching and drifting of TiB_2 grains in the melt. At the same time, the edges of TiB_2 grains are attached by the melt, resulting in Ti–B bond breakage. In addition, the attacked regions are oxidized, and TiO_2 is formed. Further examination of frozen melts on the samples reveals a mullite type of aluminum boride $(Al_2O_3)0.74\%(B_2O_3)0.26\%$ formation. Metallic additives are thus not advisable to maintain the TiB_2 structural integrity.

On the other hand, the TiB_2 coating (thickness 10 µm) on Mo substrate prepared in FLiNaK was tested for corrosion behavior in molten aluminum at 720 °C for 168 h [54]. No trace of corrosion on the TiB_2 layer was observed after the corrosion tests (wear rate 0 mm/year). Moreover, the TiB_2 was thoroughly wetted with molten aluminum.

Table 1 Energy-saving through wettable cathodes

Based on	Energy saving	Comments	References
Replacing conventional cathodes in a cell with 14 kWh/kg Al	1.5 kWh/kg Al	Referring to the steps taken by RUSAL to replace carbon cathode with wettable TiB_2 cathode	[62]
Replacing conventional cathodes by carbon cathode coated with TiB_2 layer in a cell with 14 kWh/kg Al	0.4 kWh/kg Al	Industrial cell (300 kA), with a voltage drop up to 0.05 V (improving current efficiency by 2%)	[63]
Replacing conventional cell (with specific energy consumption 15 kWh/kg Al) with VEC (*with TiB_2 cathodes and inert anodes*)	4 kWh/kg Al	Can reduce global warming potential by 30%	[64]
Replacing conventional cathodes by carbon cathode coated with TiB_2 layer in a drained cathode cell with 14.3 kWh/kg Al	2.3 kWh/kg Al	Reduces the greenhouse gas emission by 2.3 t CO_2e/t aluminum	[65]

Industrial Trials Using TiB_2 Cathodes

TiB_2 cathodes have shown some promising results during industrial trials conducted by Chinese researchers and have been well described in the review [5]. Ren et al. [55] performed industrial trials on carbon cathode blocks coated with TiB_2/C compound layer (using vibration molding process) in a 300 kA aluminum reduction cell at Yichuan aluminum smelter plant. It was estimated that the voltage drop was up to 50 mV less than the conventional cells. Thus, saving energy up to 0.4 kWh/kg Al and improving the current efficiency by 1–2.5%. Titanium concentration in primary aluminum produced was around 0.0025 wt%. Authors suggest that the TiB_2-based coating cathode blocks could prolong cell life, improve current efficiency, and save energy. Ban et al. [56] reported that the TiB_2/C composite cathode coating solidified under ambient temperature performed stably in a 300 kA aluminum reduction cell and the average voltage drop was lessened up to 10.3 mV. The current efficiency of the cell was increased by 0.81%. The expected life of the TiB_2/C composite cathode coating could be about 30 months. Tabereaux et al. [57] tested mushroom-shaped TiB_2/graphite composite cathodes in a 70 kA aluminum reduction cell for four to five months at the Kaiser Mead smelter. They reported that when the cathode material was intact, the energy consumption of the cell was 8% lower than a conventional cell. However, with time, a breakage in TiB_2/graphite cathode elements was observed causing cathode lining erosion. TiB_2-based coatings have shown excellent wear resistance when tested in cells with current loads ranging from 100 to 300 kA. Cathode wear monitoring data showed that the cathode erosion was reduced to less than 4 mm/year while using TiB_2-based coatings [57]. Feng et al. [58] tested TiB_2 coating cathodes in 1.35 kA drained cathode reduction cells, where the cathode had an inclination angle of 10°. After 100 h of electrolysis, the cell was still performing steadily and the current efficiency was 86% which was approaching the current efficiency of a conventional cell. The TiB_2 coatings showed no damage and had a low dissolution speed of about 1.0 g/h.m^2 in the electrolyte. TiB_2/C cathodes were used in 92 kA drained cathode reduction cell of Comalco Aluminium Ltd. The lowest energy consumption was reported to be 12.8 kWh/kg Al [59]. However, no significant research was conducted on cathode drained cells and has failed to reach the expectation and industrial adoption [60].

Environmental and Economic Impact

The importance of inert anodes for aluminum electrolysis is well known. A new cell design with vertically placed electrodes enables energy savings and eliminates CO_2 emissions from the electrolysis. Such a cell design should include inert anodes and wettable cathodes. TiB_2 material has been considered a suitable cathode material due to its excellent wettability towards aluminum and good resistance towards electrolyte penetration, enabling a molten aluminum cathode surface. The TiB_2 also works at low ACDs, reducing cell potential and eventually reducing specific energy consumption. Using VEC can reduce the operating cost by up to 6% compared to the conventional cell [61]. The following table includes the energy savings from using wettable cathodes. RUSAL replaced graphite cathodes with wettable TiB_2 cathodes in conventional Hall–Heroult cells, which enabled reduction in specific energy consumption by up to 1.5 kWh/kg Al. Norgate et al. [64] mentioned that the specific energy consumption required for aluminum could be reduced up to 30% if conventional aluminum reduction cells are replaced by VEC equipped with wettable TiB_2 cathodes and inert anodes (Table 1).

Conclusion

TiB_2 wettable cathodes have been studied for several decades due to their attractive properties and good wettability with molten aluminum, which is suitable for replacing non-wetted

cathodes and becoming an integral part of VEC with inert anodes. TiB_2 cathodes can be synthesized using sintering, electrodeposition, plasma spray, CVD, etc. Using sintering/hot press techniques, the processing cost of TiB_2 is not on par with the manufacturing of cathodes, making it economically unsuitable for fabricating the cathodes. Although, TiB_2 deposition is an economically attractive process; however, there are a few obstacles, such as finding a suitable substrate (with a thermal expansion coefficient closer to TiB_2), finding an environmentally friendly electrolyte that does not release harmful byproducts, achieving fully dense and non-porous deposit, and finally, a coating resistant to electrolyte penetration. According to the literature, the electrodeposition should be conducted at low cathode current densities and low deposition temperatures to avoid microcracks and obtain non-porous coating.

Moreover, the TiB_2 layer should have good wettability towards aluminum, which helps to increase cathode lifespan. The TiB_2 surface should be free of oxide layers as these layers act as barriers between molten aluminum and TiB_2, further influencing the wettability. It is preferred to use low-temperature electrolytes for a longer cell lifetime.

Funding Open access funding provided by NTNU Norwegian University of Science and Technology (incl St. Olavs Hospital - Trondheim University Hospital).

Declarations

Conflict of interest On behalf of all authors, the corresponding author states that there is no conflict of interest.

References

1. Saevarsdottir G, Kvande, H, Welch, BJ (2020) Reducing the carbon footprint: aluminium smelting with changing energy systems and the risk of carbon leakage. In: Tomsett A (ed) Light metals 2020. Springer, Cham, pp. 726−734
2. Saevarsdottir G, Kvande H, Welch BJ (2020) Aluminum production in the times of climate change: the global challenge to reduce the carbon footprint and prevent carbon leakage. JOM 72:296–308
3. Kvande H, Haupin W (2001) Inert anodes for Al smelters: energy balances and environmental impact. JOM 53:29–33
4. Brown C (2001) Next generation vertical electrode cells. JOM 53:39–42
5. Li J, Lü X, Lai Y, Li Q, Liu Y (2008) Research progress in TiB_2 wettable cathode for aluminum reduction. JOM 60:32–37
6. Sørlie M, Øye HA (2010) Cathodes in aluminium electrolysis, 3rd edn. Aluminium-Verlag Marketing & Kommunikation GmbH, Düsseldorf
7. Koh YH, Lee SY, Kim HE (2001) Oxidation behavior of titanium boride at elevated temperatures. J Am Ceram Soc 84:239–241
8. Welch BJ, Hyland MM, James BJ (2001) Future materials requirements for the high-energy-intensity production of aluminum. JOM 53:13–18
9. Panda KB, Ravi Chandran KS (2006) Determination of elastic constants of titanium diboride (TiB_2) from first principles using FLAPW implementation of the density functional theory. Comput Mater Sci 35:134–150
10. Kang SH, Kim DJ (2001) Pressureless sintering and properties of titanium diboride ceramics containing chromium and iron. J Am Ceram Soc 84:893–895
11. Jensen MS, Einarsrud M, Grande T (2007) Preferential grain orientation in hot pressed TiB_2. J Am Ceram Soc 90:1339–1341
12. Heidari H, Alamdari H, Dubé D, Schulz R (2012) Investigating the potential of TiB_2–based composites with Ti and Fe additives as wettable cathode. Adv Mater Res 409:195–200
13. Mazza B, Serravalle G, Fumagalli G, Brunella F (1987) Cathodic behavior of titanium diboride in aluminum electrolysis. J Electrochem Soc 134:1187–1191
14. Xi L, Kaban I, Nowak R, Korpała B, Bruzda G, Sobczak N, Mattern N, Eckert J (2015) High-temperature wetting and interfacial interaction between liquid Al and TiB_2 ceramic. J Mater Sci 50:2682–2690
15. Balci O, Burkhardt U, Schmidt M, Hennicke J, Yağcı MB, Somer M (2018) Densification, microstructure and properties of TiB_2 ceramics fabricated by spark plasma sintering. Mater Charact 145:435–443
16. Zou K, Zou J, Deng C, Liu M, Liu X, Zhao R, Li S, Zhu R, Gao D (2021) Preparation and properties of supersonic atmospheric plasma sprayed TiB_2−SiC coating. Trans Nonferrous Met Soc China 31:243–254
17. Wendt H, Reuhl K, Schwarz V (1992) Cathodic deposition of refractory intermetallic compounds from FLINAK melts Part II: Preparative cathodic deposition of TiB_2 and ZrB_2 and coatings thereof. J Appl Electrochem 22:161–165
18. Wendt H, Reuhl K, Schwarz V (1992) Cathodic deposition of refractory intermetallic compounds from FLINAK-melts I. Voltammetric investigation of Ti, Zr, B, TiB_2, and ZrB_2. Electro Acta 37:237–244
19. Guven A, Friedrich B (2009) Electrochemical titanium diboride (TiB_2) synthesis from fluoride melts. Proc EMC 2009:1313
20. Li J, Li B (2007) Preparation of the TiB_2 coatings by electroplating in molten salts. Mater Lett 61:1274–1278
21. Makyta M, Danek V, Haarberg GM, Thonstad J (1996) Electrodeposition of titanium diboride from fused salts. J Appl Electrochem 26:319–324
22. Yvenou E, Davis B, Guay D, Roué L (2021) Electrodeposited TiB_2 on graphite as wettable cathode for Al production. J Am Ceram Soc 104:1247–1254
23. Ozkalafat P, Sireli GK, Timur S (2016) Electrodeposition of titanium diboride from oxide based melts. Surf Coat Technol 308:128–135
24. Huang Y, Wang Y, Zhang X, Wang H, Li Q (2019) Preparation of wettable TiB_2-TiB/Ti cathode by electrolytic boronizing for aluminum electrolytic. J Cent South Univ 26:2681–2687

25. Kartal G, Timur S (2013) Growth kinetics of titanium borides produced by CRTD-Bor method. Surf Coat Technol 215:440–446
26. Vardelle A, Moreau C, Akedo J, Ashrafizadeh H, Berndt CC et al (2016) The 2016 thermal spray roadmap. J Therm Spray Technol 25:1376–1440
27. Peng RZ, Xie G, Hou YQ, Tian L, Yu XH (2014) Microstructure and property of plasma sprayed TiB_2 wettable coatings on carbon cathodes. Adv Mater Res 881:1580–1583
28. Ananthapadmanabhan PV, Sreekumar KP, Ravindran PV, Venkatramani N (1993) Effect of oxygen pick-up on the properties of plasma sprayed titanium diboride coatings. Thin Solid Films 224:148–152
29. Yvenou E, Bily A, Ettouil FB, Dolatabadi A, Davis B, Guay D, Moreau C, Roue L (2021) TiB_2 Deposited on graphite by suspension plasma spray as Al wettable cathode. J Therm Spray Tech 30:1535–1543
30. Berger M (2002) Thick physical vapour deposited TiB_2 coatings. Surf Eng 18:219–223
31. Choy KL (2003) Chemical vapour deposition of coatings. Prog Mater Sci 48:57–170
32. Moers VK (1931) Die Reindarstellung hochschmelzender Carbide, Nitride und Boride nach dem Aufwachsverfahren und Beschrebung einiger ihrer Eigenschaften. Z Anorg Allg Chem 198:243–261
33. Besmann TM, Spear KE (1975) Morphology of chemical vapor deposited titanium diboride. J Cryst Growth 31:60–65
34. Caputo AJ, Lackey WJ, Wright IG (1985) Chemical vapor deposition of erosion resistant TiB_2 coatings. J Electrochem Soc 132:2274–2280
35. Beckloff BN, Lackey WJ (1999) Process–structure–reflectance correlations for TiB_2 films prepared by chemical vapor deposition. J Am Ceram Soc 82:503–512
36. Becht JGM, van Dieten VEJ, Schoonman J (1991) Chemical vapor deposition of TiB_2 for TiN-TiB_2 laminar composites. Mater Manuf Processes 6:423–432
37. Pierson HO, Randich E (1978) Titanium diboride coatings and their interaction with the substrates. Thin Solid Films 54:119–128
38. Namini AS, Gogani SNS, Asl MS, Farhadi K, Kakroudi MG, Mohammadzadeh A (2015) Microstructural development and mechanical properties of hot pressed SiC reinforced TiB_2 based composite. Int J Refract Met Hard Mater 51:169–179
39. Zhao G, Huang C, Liu H, Zou B, Zhu H, Wang J (2014) Microstructure and mechanical properties of TiB_2–SiC ceramic composites by Reactive Hot Pressing. Int J Refract Met Hard Mater 42:36–41
40. Wang Z, Li H, Zhang C, Xue J, Liu X, Li X, He D (2021) The role of TiB_2 particles in the creep and penetrating resistance of graphite-based composite. Ceram Int 47:12096–12103
41. Fei J, Wang W, Ren A, Ji Y, Zhou J, Zhu M (2014) Mechanical properties and densification of short carbon fiber-reinforced TiB_2/C composites produced by hot pressing. J Alloys Compd 584:87–92
42. Lu J, Fang J, Li Q, Lai Y (2004) Effect of TiB_2 content on resistance to sodium penetration of TiB_2/C cathode composites for aluminium electrolysis. J Cent South Univ Technol 11:400–404
43. Li J, Lu X, Li Q, Lai Y, Yang J (2006) Electrical resistivity of TiB_2/C composite cathode coating for aluminum electrolysis. J Cent South Univ Technol 13:209–213
44. Smith CS (1948) Grains, phases and interfaces: an interpretation of microstructure. Trans AIME 175:15–51
45. Heidari H, Alamdari H, Dubé D, Schulz R (2012) Interaction of molten aluminum with porous TiB_2-based ceramics containing Ti-Fe additives. J Eur Ceram Soc 32:937–945
46. Raj SC, Skyllas-Kazacos M (1992) Electrochemical studies on wettability of sintered TiB_2 electrodes in aluminium electrolysis. Electrochim Acta 37:1395–1401
47. Watson KD, Toguri JM (1991) The Wettability of carbon/TiB_2 composite materials by aluminum in cryolite melts. Metall Trans B 22:617–621
48. Dorward RC (1982) Aluminum penetration and fracture of titanium diboride. J Am Ceram Soc 65:C6
49. Weirauch DA, Krafick WJ, Ackart G, Ownby PD (2005) The wettability of titanium diboride by molten aluminium drops. J Mater Sci 40:2301–2306
50. Jensen MS, Pezzotta M, Zhang ZL, Einarsrud MA, Grande T (2008) Degradation of TiB_2 ceramics in liquid aluminum. J Eur Ceram Soc 28:3155–3164
51. Kubiňáková E, Benköová M, Veteška P, Bača L, Híves J (2020) Surface characterisation and wettability of titanium diboride by aluminium at low temperature. Adv Appl Ceram 119:22–28
52. Devyatkin SV, Kaptay G (2000) Chemical and electrochemical behavior of titanium diboride in cryolite-alumina melt and in molten aluminum. J Solid State Chem 154:107–109
53. Kontrík M, Šimko F, Galusková D, Nosko M, Bizovská V, Hičák M, Galusek D, Rakhmatullin A, Korenko M (2020) A corrosion mechanism of titanium diboride in $KF-AlF_3-Al_2O_3$ melt. J Eur Ceram Soc 170:108646
54. Rybakova N, Souto M, Martinz HP, Andriyko Y, Artner W, Godinho J, Nauer GE (2009) Stability of electroplated titanium diboride coatings in high-temperature corrosive media. Corros Sci 51:1315–1321
55. Ren B, Xu J, Shi Z, Yungang B, Dai S, Wang Z, Gao B (2007) Application of TiB_2 coating cathode blocks made by vibration molding for 300 kA aluminum reduction cells. In: Sorlie M (ed) Light metals 2007. TMS, Warrendale, PA, pp 1047–1050
56. Ban Y, Shi Z, Wang Z, Kan H, Yang S, Cao X, Qiu Z (2007) Application of TiB_2/C composite cathode coating solidified at ambient temperature in 300 kA prebaked aluminum reduction cell. In: Sorlie M (ed) Light metals 2007. TMS, Warrendale, PA, pp 1051–1054
57. Tabereaux A, Brown J, Eldridge I, Morgan W, Stewart D, McMinn C, Alcorn T, Rozelle V, Thorson D, Sprecher M, Hullett B, Warren C (1998) Operational performance of 70 kA prebake cells retrofitted with TiB_2-G cathode elements. In: Welch BJ (ed) Light metals 1998. TMS, Warrendale, PA, pp 257–264
58. Feng NX, Qi XQ, Peng JP (2005) Electrolysis test of 1.35 kA drained cathode reduction cell with TiB_2-coated cathode. Chin J Nonferrous Met 15:2047–2053
59. Kvande H (1999) The 6th Australasian Aluminium smelting technology conference and workshop. Light Met Age 2:68–71
60. Feng N, Tian Y, Peng J, Wang Y, Qi X, Tu G (2010) New cathodes in aluminum reduction cells. In: Johnson JA (ed) Light metals 2010. TMS, Warrendale, PA, pp 523–526
61. Keniry J (2001) The economics of inert anodes and wettable cathodes for aluminum reduction cells. JOM 53:43–47
62. Galevskiy GV, Rudneva VV, Galevskiy SG, Komroni M, Gordiyevsky OI (2020) The use of titanium diboride to protect the cathodes of aluminum electrolysis cells. IOP Conf Ser: Mater Sci Eng 866:012007
63. Shi Z, Xu J, Ren B, Ban Y, Wang Z (2007) Tests of various graphitic cathode blocks materials for 300 KA aluminum reduction cells. In: Sorlie M (ed) Light metals 2007. TMS, Warrendale, PA, pp 849−852
64. Norgate TE, Jahanshahi S, Rankin WJ (2007) Assessing the environmental impact of metal production processes. J Clean Prod 15:838–848
65. Norgate T, Jahanshahi S (2011) Reducing the greenhouse gas footprint of primary metal production: where should the focus be? Miner Eng 24:1563–1570